

Vector Flow Mapping in the Brain

Abstract. The two highest death rate diseases are coronary artery disease (CAD) and stroke. In clinical practice, visualization of blood flow inside brain vessels are essential for the diagnosis and treatment for abnormal vessel diseases. Abnormal vessels can be detected and visualized with certain approaches like magnetic resonance imaging (MRI) and computed tomography (CT). This paper provides an approach to acquire vector flow information from source magnetic resonance perfusion images. It is a practical approach to acquire flow information from raw brain MR perfusion images. This could be widely implemented to diagnosis of abnormal vessel diseases.

1 Introduction

The two highest death rate diseases are coronary artery disease (CAD) [1] and stroke [2]. In Western society, about 80% of strokes are caused by focal cerebral ischemia due to arterial occlusion [3]. In clinical practice, detection and visualization of blood flow inside brain vessels is essential for the diagnosis and treatment for abnormal vessel diseases. Abnormal vessels can be detected and visualized with certain approaches such as magnetic resonance imaging (MRI) and computed tomography (CT).

Perfusion imaging has flourished in the past two decades [4]. The noninvasive method Artrial Spin Labeling (ASL) [5] and the invasive method angiography [6] both work well with perfusion imaging. Dynamic Susceptibility Contrast (DSC) perfusion MRI [7] also plays an important role in ischemic stroke [8], and other arterial diseases such as hypertensive cerebrovascular disease [9] and brain tumor [10].

Monitored by a series of T2- or T2*- weighted MR images [11], DSC perfusion MRI begins with contrast, usually gadolinium chelate, injected intravenously. Due to its paramagnetic properties, the contrast creates a local magnetic field distortion around vessels [3], which makes the signal of MR images enhanced through the trajectory of contrast. By measuring the signal intensity of certain areas, images that depict blood flow inside vessels will then be acquired.

This paper provides an approach to vector flow mapping in DSC perfusion MR images of the brain. It shows a way to acquire flow information from raw MR Perfusion images. This approach could be widely implemented to diagnosis of abnormal vessel diseases. The outline of this paper is briefly introduced as follows. The computation of contrast concentration will be introduced in Section 2.1. The gradient computation and flow vector acquisition will be explained in Section 2.2. The color visualization method will be described in Section 2.3. The results and discussion will be given in Section 3. The conclusion will be given in Section 4.

2 Methods

2.1 Contrast Computation

Term Convention In anatomy terms, the three orthogonal plane for human body are coronal plane, median (sagittal) plane and transverse plane [12]. A right-handed three-dimensional Cartesian coordinate system to denote the transverse plane as x-y plane, x-z for coronal plane and y-z for median.

Contrast Concentration Computation DSC Perfusion MRI begins with the contrast, usually to be gadolinium chelate, injected intravenously. Before the gadolinium contrast arrives, the magnetic field would be steady. During its arrival, it creates a local distortion where it flows through. Tissues with high fat content appear bright and vessels filled with water appear dark in the DSC Perfusion MR images. For every voxel, The greyscale of the image is proportional to baseline signal intensity (S_0) before contrast arrives, and proportional to combination signal intensity ($S(t)$) during passage of the gadolinium bolus at the time point t [13].

The concentration of gadolinium is proportional to negative logarithm of relative signal intensity represented as Eq.(2) [14]

$$C(t) = -\frac{k}{TE} \ln\left(\frac{S(t)}{S_0}\right) \quad (1)$$

In Eq. 1, $C(t)$ is the concentration of contrast in a given voxel, S_0 is the baseline signal intensity and $S(t)$ is the signal intensity at time point t. During passage of the gadolinium bolus, $S(t)$ is usually greater than S_0 . Therefore, all negative results are caused by noise or over estimation of S_0 . TE is echo time, and k is an arbitrary parameter to adjust $C(t)$ to a proper magnitude. The Eq. 1 is semi-quantitative.

The calculation of baseline signal intensity S_0 is disturbed by noise before the arrival time (t_0 , AT) [11]. Also, S_0 is differentiated in voxels. Therefore the calculation of S_0 should be dense and local. For a given voxel, it is feasible to estimate t_0 . An easy method is to acquire the signal intensity at t_{peak} to be S_{peak} , then set a threshold proportional to S_{peak} to find the last time point t_1 the intensity below the threshold.

The MR images are sampled at several transverse layers, and the distance between each layer is about 5 to 6mm. The distance between layers is usually greater than the minimum resolution of the image (pixel size, usually to be 1mm). In order to build a cubic voxel, linear interpolation is introduced to refine the scaling of $C(t)$ in z direction:

$$C_{voxel}(i) = \alpha * C_{l-1} + (1 - \alpha) * C_l \quad (2)$$

$$\alpha = (z_l - m)/(z_l - z_{l-1}) \quad (3)$$

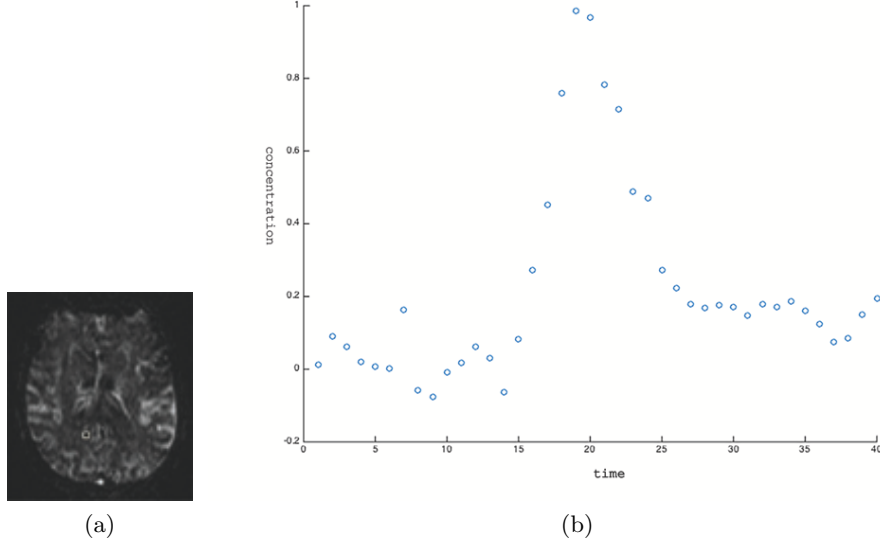


Fig. 1: (a) Selected pixel in raw MR image. (b) Contrast concentration in a given voxel by time sequence.

In Eq. 2, $C_{\text{voxel}}(i)$ stands for the concentration at the i^{th} x-y plane after interpolation, m is for the distance between the new layer and the l^{th} layer, and α is the linear interpolation parameter. A dense map of C_{voxel} could then be generated.

2.2 Gradient Computation and Flow Vector Acquisition

ROI Selection The regions of interest (ROI) are binary masks on x-y layers and are semi-automatically generated. By adjusting the brightness and contrast of the Perfusion MRI images and setting up greyscale thresholds [15], raw ROIs are generated on each layer (Fig. 2 (a)). A morphological closing method [10] with radius 1 disk as parameter is introduced to smooth harsh edges and fill inside points. As this method is not a iterative function, some residues skull stripping are removed by hand.

For further refinements of ROI, the derivative of concentration by time ($\frac{d}{dt}C(t)$) is taken into consideration. Because that $\frac{d}{dt}C(t)$ reaches its peak during or after the arrival of labeled blood flow, it contains information on the distribution of vessels in this layer. Only the regions the contrast just arrived have a magnificent value of $\frac{d}{dt}C(t)$. The regions contrast doesn't reach and the regions reach it's peak and then degrade would have a small value of $\frac{d}{dt}C(t)$. A threshold is set to alter the mask to a proper shape. To some extent, proper and dense $\frac{d}{dt}C(t)$ masks are perfect depictions of perfusion flow over time (Fig. 2 (b)).

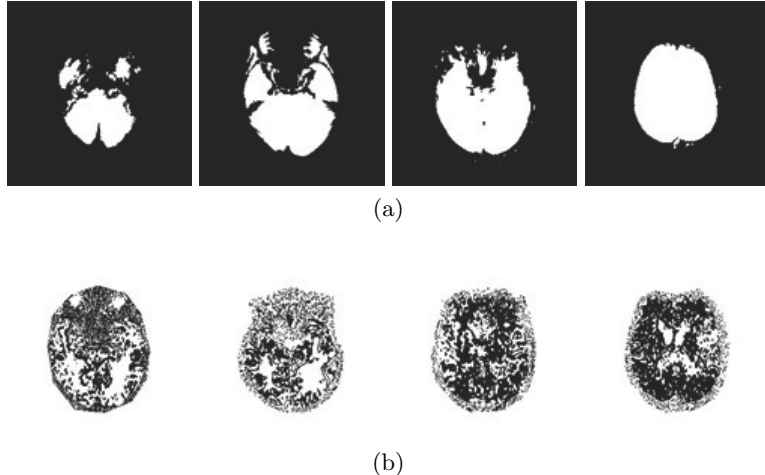


Fig. 2: (a) ROI masks generated by thresholding and morphological closing. (b) ROI masks of $\frac{d}{dt}C(t)$.

Gradient Computation and Flow Vector Acquisition The computation of spacial gradient is implemented on three orthogonal directions, x, y and z. For each voxel, the gradient \mathbf{G} is with 3 components G_x , G_y and G_z . The temporal information is represented by computing the changing in \mathbf{G} by time. The changing in magnitude (ΔM) is defined in Eq. 4.

$$\Delta M = \|\mathbf{G}_1\|_2 - \|\mathbf{G}_0\|_2 \quad (4)$$

ΔM represents for the magnitude changing of gradient vector, and \mathbf{G}_1 is the gradient vector of the next time point of \mathbf{G}_0 . Once we acquired the orientation of flow vector \mathbf{K} , the flow vector \mathbf{F} could be represented in Eq. 5.

$$\mathbf{F} = \Delta M \cdot \mathbf{K} \quad (5)$$

However, the orientation of the flow vector is a thought provoking issue and is still an open question. One way is to take the subtraction of two gradient vectors ($\mathbf{G}_1 - \mathbf{G}_0$) as the new orientation. Another way is simply using the direction of the gradient vector \mathbf{G}_1 . The first way works well when the absolute value of ΔM is big enough. It means that the gradient changing on magnitude is sizable. But when the changing on magnitude is small, like in the cases of magnificent blood flow orientation changing in arteries [16], the second way works better. In this paper, we took the second way to represent the orientation.

2.3 Visualization Methods

Visualization by greyscale is done by mapping the data to 8-bit images after normalization. The color encoding method of RGB visualization is presented in

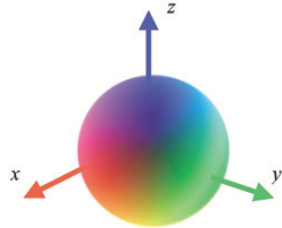


Fig. 3: Directional color encoding method represented by sphere [17].

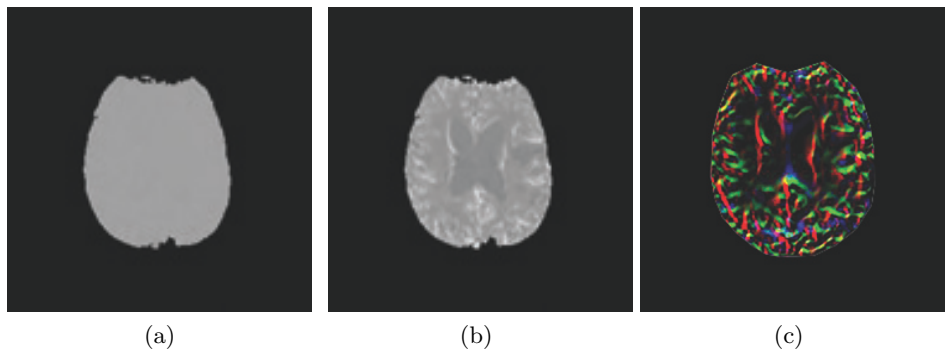


Fig. 4: (a) Greyscale visualization of concentration at time point 0 (background signal). (b) Greyscale visualization of concentration at peak. (c) 8-bit (for each channel) RGB Coloring visualization of concentration at peak.

Fig. 3. As there are three orthogonal components of \mathbf{F} in each voxel, the x, y and z component of \mathbf{F} is respectively corresponded to RGB color space in red, green and blue order [17] [18]. For both greyscale and RGB method, black is selected to be the background color. For figures generated by the MATLAB function `imagesc` [19], the color-mapping method `jet` is used. A visualization example of x-y layer is shown in Fig.4.

3 Result

The results of the color visualization of concentration are shown in Fig. 6. By mapping the gradient vectors in to RGB images, the main direction in each voxel is represented by its color. The magnitude of each color channel represents the gradient magnitude in that direction. Mostly the brighter a voxel is, the more blood flow is arrived. The darker it is, the less flow is arrived.

The sum flow (\mathbf{F}) is defined in Eq. 5, the Increasing Flow (\mathbf{IF}) is defined in Eq. 6.

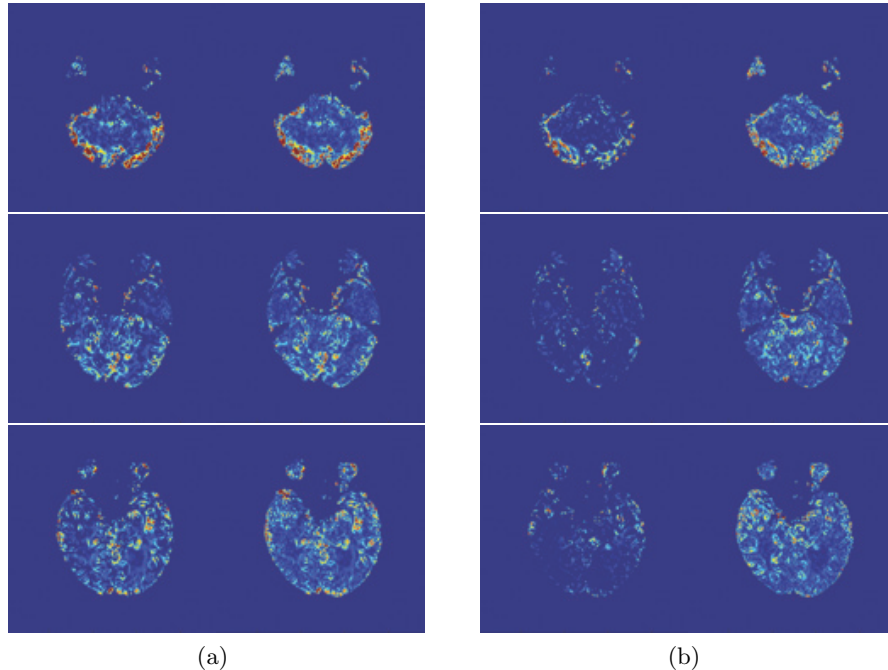


Fig. 5: (a): magnification of increasing flow (left column) and magnification of sum flow (right column) at peak. (b): magnification of increasing flow and magnification of sum flow after peak.

$$\mathbf{IF} = \begin{cases} \Delta M \cdot \mathbf{K} & \Delta M > 0 \\ \mathbf{0} & \Delta M \leq 0 \end{cases} \quad (6)$$

and the decreasing flow (\mathbf{DF}) is defined naturally in Eq. 7.

$$\mathbf{DF} = \mathbf{F} - \mathbf{IF} \quad (7)$$

The Fig. 5 demonstrates the magnitude of \mathbf{IF} and \mathbf{F} . The left column shows $\|\mathbf{IF}\|_2$ and $\|\mathbf{F}\|_2$ Before peak, while the right shows $\|\mathbf{IF}\|_2$ and $\|\mathbf{F}\|_2$ after peak. Compared to the right column, $\|\mathbf{IF}\|_2$ is very close to $\|\mathbf{SF}\|_2$ before peak. It means that \mathbf{IF} is the main component of \mathbf{F} before peak, and \mathbf{IF} decreases gradually after peak. The magnitude of \mathbf{DF} increases on a equivalent level as \mathbf{IF} after peak. Because of that, \mathbf{F} maintains on a high level for a considerable time after peak. Furthermore, the flow is mainly coming to this layer during time-to-peak(TTP), and propagating to other layers after peak. \mathbf{IF} only depicts the front of flow and ignore the decreasing of concentration. As the increasing of blood flow are mostly in arteries, \mathbf{IF} is a great representation to the arterial blood flow.

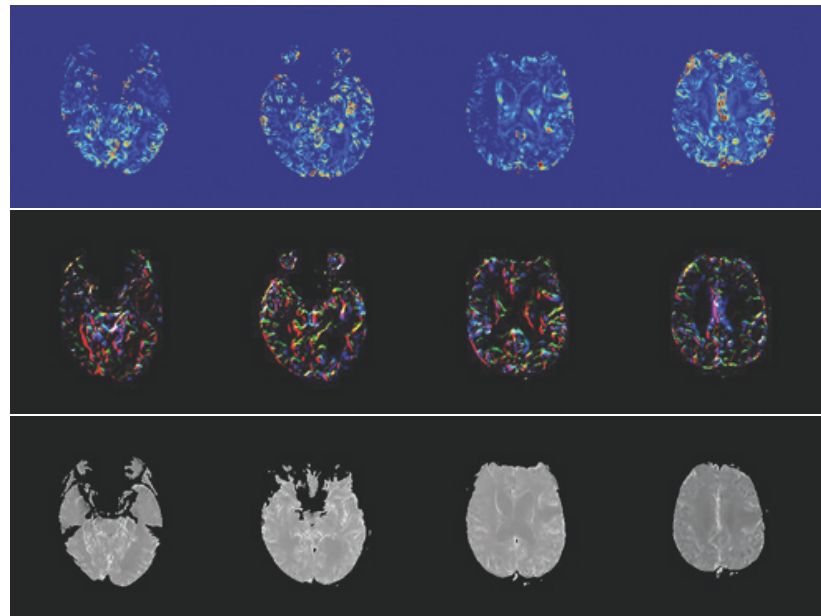
4 Conclusion

We have introduced the method of vector flow mapping of Perfusion MRI in this paper. It is a practical approach to acquire flow information from raw brain MR Perfusion images. The flow is depicted by its changing on magnitude and flow front. The changing on magnitude shows the amount of cerebral blood flow (CBF), and the flow front curves the orientation of CBF. Based on our method, other medical parameters like cerebral blood volume (CBV), mean transit time (MTT), time to peak (TTP) and time of arrival (t_0 , AT) [11] could also be acquired.

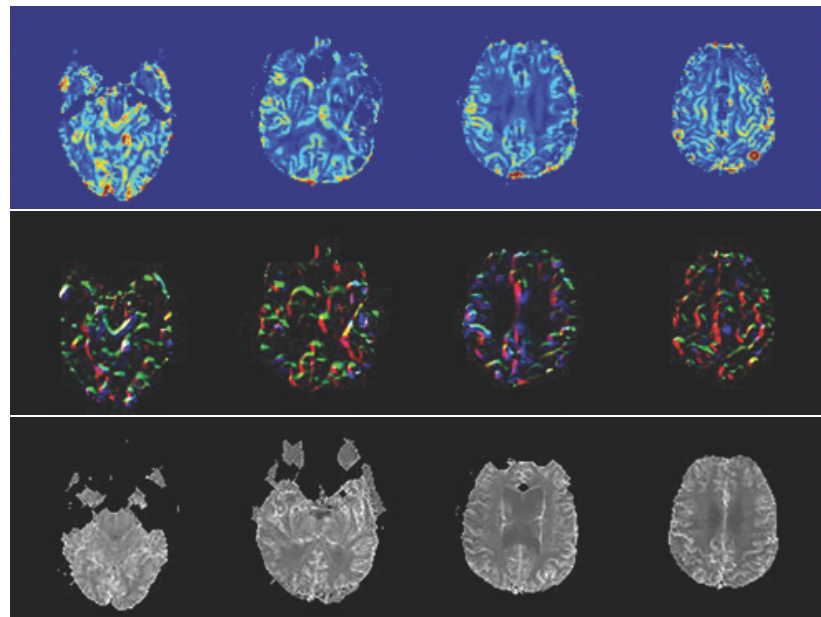
Another issue is to further improve automatic prediction algorithm [20] to generate probable disease regions of cerebral abnormal vessel diseases patients based on the map of CBF. To accomplish this task, machine learning methods should also be introduced. Although further quantitative study and statistical analysis on a larger dataset are needed, the result still shows the promised application future of the flow mapping technique. This could be widely implemented to automatic diagnosis on stroke and other abnormal vessel diseases. In addition, with 3D modeling software, reconstruction of the entire blood circulatory system is definitely feasible.

References

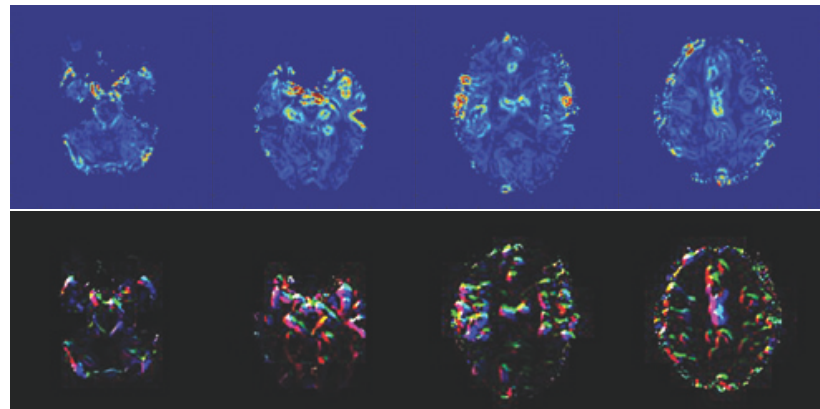
1. McCullough, P.A.: Coronary artery disease. Clinical Journal of the American Society of Nephrology **2** (2007) 611–616

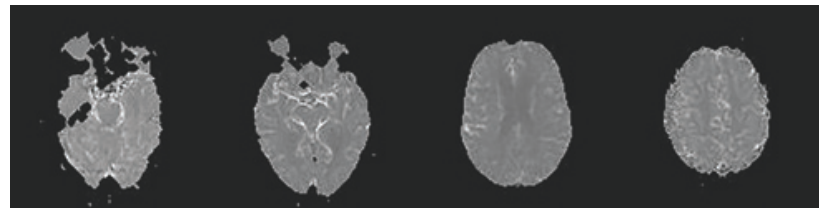


(a) Patient 1

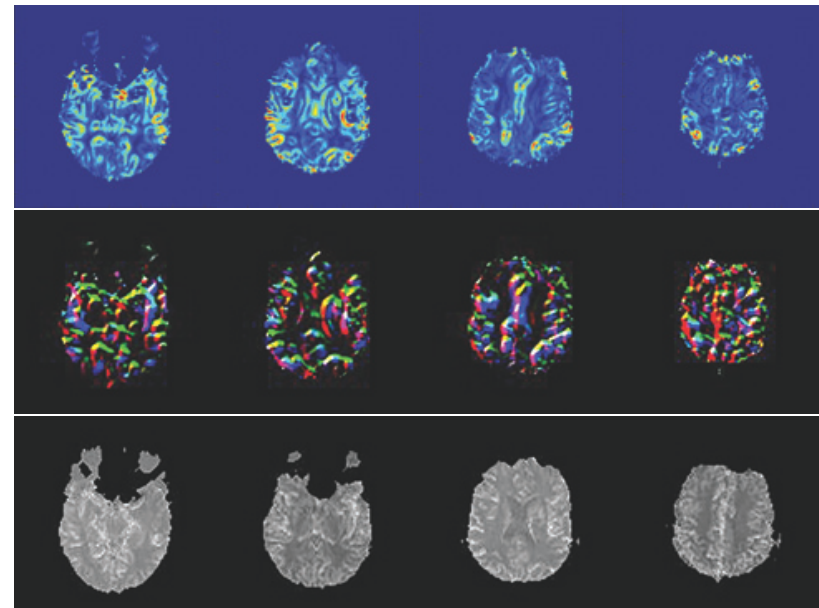


(b) Patient 2

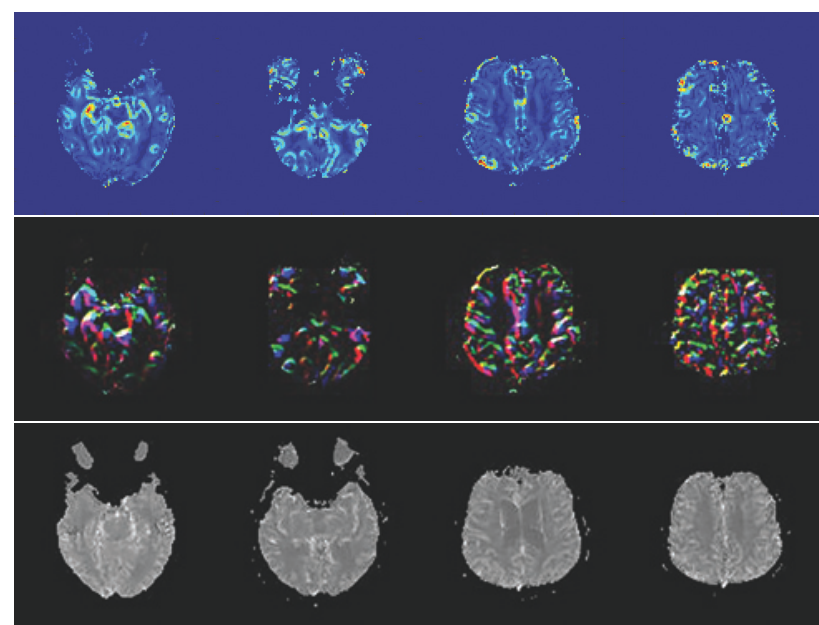




(d) Patient 3



(e) Patient 4



(f) Patient 5

Fig.6: Color visualization result of the brain flow in different layers. Top row: magnification of flow vector. Medium row: propagating front of blood flow. Below row: contrast concentration at peak time.

2. Feigin, V.L., Lawes, C.M., Bennett, D.A., Anderson, C.S.: Stroke epidemiology: a review of population-based studies of incidence, prevalence, and case-fatality in the late 20th century. *The Lancet Neurology* **2** (2003) 43–53
3. Essig, M., Shiroishi, M.S., Nguyen, T.B., Saaqe, M., Provenzale, J.M., Enterline, D., Anzalone, N., Dörfler, A., Rovira, Å., Wintermark, M., et al.: Perfusion mri: the five most frequently asked technical questions. *AJR. American journal of roentgenology* **200** (2013) 24
4. Liebeskind, D.S.: Imaging the future of stroke: I. ischemia. *Annals of Neurology* **66** (2009) 574–590
5. Frank, L.R., Lu, K., Wong, E.C.: Perfusion tensor imaging. *Magnetic resonance in medicine* **60** (2008) 1284–1291
6. Scalzo, F., Liebeskind, D.S.: Perfusion angiography in acute ischemic stroke. (2016)
7. McGehee, B.E., Pollock, J.M., Maldjian, J.A.: Brain perfusion imaging: how does it work and what should i use? *Journal of Magnetic Resonance Imaging* **36** (2012) 1257–1272
8. van der Worp, H.B., van Gijn, J.: Acute ischemic stroke. *New England Journal of Medicine* **357** (2007) 572–579
9. Meng, Q., Sun, X.: Advances of magnetic resonance perfusion imaging in hypertensive cerebrovascular diseases. *Chin J Magn Reson Imaging* **2** (2011) 384–387
10. Sharma, Y., Meghrajani, Y.K.: Brain tumor extraction from mri image using mathematical morphological reconstruction. In: Emerging Technology Trends in Electronics, Communication and Networking (ET2ECN), 2014 2nd International Conference on, IEEE (2014) 1–4
11. Jahng, G.H., Li, K.L., Ostergaard, L., Calamante, F.: Perfusion magnetic resonance imaging: a comprehensive update on principles and techniques. *Korean journal of radiology* **15** (2014) 554–577
12. Vella, M.: Anatomy for strength and fitness training. New Holland Publishers (2008)
13. Kiselev, V.G.: On the theoretical basis of perfusion measurements by dynamic susceptibility contrast mri. *Magnetic Resonance in Medicine* **46** (2001) 1113–1122
14. Ostergaard, L., Johannsen, P., Høst-Poulsen, P., Vestergaard-Poulsen, P., Asboe, H., Gee, A.D., Hansen, S.B., Cold, G.E., Gjedde, A., Gyldensted, C.: Cerebral blood flow measurements by magnetic resonance imaging bolus tracking: comparison with [(15) o] h2o positron emission tomography in humans. *Journal of cerebral blood flow and metabolism: official journal of the International Society of Cerebral Blood Flow and Metabolism* **18** (1998) 935–940
15. Sahoo, P.K., Soltani, S., Wong, A.K.: A survey of thresholding techniques. *Computer vision, graphics, and image processing* **41** (1988) 233–260
16. Ku, D.N.: Blood flow in arteries. *Annual Review of Fluid Mechanics* **29** (1997) 399–434
17. Masutani, Y., Aoki, S., Abe, O., Hayashi, N., Otomo, K.: Mr diffusion tensor imaging: recent advance and new techniques for diffusion tensor visualization. *European journal of radiology* **46** (2003) 53–66
18. Vilanova, A., Zhang, S., Kindlmann, G., Laidlaw, D.: An introduction to visualization of diffusion tensor imaging and its applications. In: Visualization and Processing of Tensor Fields. Springer (2006) 121–153
19. Smith, S.T.: MATLAB: advanced GUI development. Dog ear publishing (2006)
20. Scalzo, F., Hao, Q., Alger, J.R., Hu, X., Liebeskind, D.S.: Regional prediction of tissue fate in acute ischemic stroke. *Annals of biomedical engineering* **40** (2012) 2177–2187